present resonance Hamiltonian to a complete set of basis states and yields further significant improvements in the description of $S = {}^1/_2, {}^3/_2$, and ${}^7/_2$ states as well as spin crossover phenomena.

Acknowledgment. I thank D. A. Case, P. Yip, E. Munck, J. Girerd, V. Papaefthymiou, J. Gaillard, and B. H. Huynh for valuable discussions and the National Institutes of Health (Grant GM39914) for financial support. I also thank J. P. Desclaux for providing the Racah coefficient and matrix diagonalization routines.

Contribution from the Department of Molecular Biology, MB1, Research Institute of Scripps Clinic, La Jolla, California 92037

Exchange Coupling and Resonance Delocalization in Reduced $[Fe_4S_4]^+$ and $[Fe_4Se_4]^+$ Clusters. 2. A Generalized Nonlinear Model for Spin-State Energies and EPR and Hyperfine Properties

Louis Noodleman

Received April 16, 1990

I develop a generalized nonlinear model for the spin states of reduced $[Fe_4S_4]^+$ and $[Fe_4Se_4]^+$ clusters. This model is an extension of that described in the previous paper and allows the internal electron transfer within the mixed-valence pair to couple together a larger set of basis states. The consequences of this model for the energies and properties of various states with spin $S = {}^1/_2$, ${}^3/_2$, and ${}^7/_2$ are explored. For a range of parameters similar to that used previously, we find that the lowest $S = {}^3/_2$ state appears in much closer proximity to the lowest $S = {}^1/_2$ state over an extended range of the $\alpha = J_2/J_1$ parameter compared with the preceding linear model. Such a near proximity of $S = {}^1/_2$ and ${}^3/_2$ is consistent with the statistical mixtures of these states often found in reduced $[Fe_4S_4]^+$ and $[Fe_4Se_4]^+$ clusters. The observed crossing points among $S = {}^1/_2$, ${}^3/_2$, and ${}^7/_2$ are consistent with the observed coexistence of these three states in $[Fe_4Se_4]^+$ at low temperatures. In addition to providing reasonable predictions for average g and A values for $S = {}^1/_2$ states in typical reduced 4Fe ferredoxins, the model shows how the large variation in average g values, 1.97 and 2.05, for the two different rhombic states observed in *Desulfovibrio vulgaris* hydrogenase can arise from a modest variation in $0.2 \leq \alpha \leq 0.5$ at low B/J, $3 \leq B/J \leq 2.5$. The predicted variability in average g values is a consequence of the nonlinear model; the linear model cannot give a satisfactory account of this variability. We obtain a good theoretical prediction of the small negative hyperfine constants observed by Mossbauer spectroscopy on all Fe sites in the lowest $S = {}^3/_2$ state for various clusters. The nonlinear theory gives a far better prediction of hyperfine constants for $S = {}^3/_2$ than the linear theory. The predicted theoretical A_{av} values for the Fe^{2+} and Fe^{3+} sites of the $S = {}^7/_2$ state in Se-substituted Cp ferredoxin are well represented by the nonlinear model; at least partial localization of the mixed-valence pair by extrinsic forces is indicated. The Zeeman parameter g_0' determined by EPR spectroscopy is also calculated with reasonable accuracy by the model.

I. Introduction

In the preceding paper (P 1),[1] I developed a basic model for spin-state energies and spin-dependent properties (g and A values) for reduced $[Fe_4S_4]^+$ and $[Fe_4Se_4]^+$ clusters. In this paper, I generalize this model in the most direct way possible. No new parameters are introduced, but significant improvements in the physical realism of the model are obtained by simply allowing all possible iinteractions of basis states with the same Hamiltonian as in P 1. For the same range of parameters previously used, the lowest $S = {}^3/_2$ state appears in much closer energetic proximity to the lowest $S = {}^1/_2$ state, as might be inferred empirically from the prevalence of statistical mixtures of $S = {}^1/_2$ and $S = {}^3/_2$ states in reduced $[Fe_4S_4]^+$ and $[Fe_4Se_4]^+$ clusters at very low temperatures; quantum admixtures of $S = {}^1/_2$ and ${}^3/_2$ have also been inferred from analysis of EPR and magnetization data in some cases.[2] We also obtain a good description of the small hyperfine coupling displayed by the lowest $S = {}^3/_2$ state when this is the lowest spin state overall or when there is coexistence of $S = {}^1/_2$, ${}^3/_2$, and ${}^7/_2$ low-lying states.[3] The more general model displays variability in predicted g and A values for each spin state as the location in parameter space is altered. This variability provides a reasonable explanation for the observed differences in g values of the two different rhombic states seen by EPR spectroscopy for an unusual cluster in *Desulfovibrio vulgaris* hydrogenase.[4] The hyperfine properties of the $S = {}^7/_2$ state in Se-substituted *Clostridium pasteurianum* ferredoxin are well described by the nonlinear model.

While the present nonlinear model is more accurate quantitatively than the linear model and better justified on fundamental grounds, there is also considerable value in the simpler linear model. The linear model involves only the diagonalization of 2 × 2 matrices; hence all energies are obtained as roots of quadratic equations. By contrast, the nonlinear model requires in general diagonalization of larger matrices (maximum size 10 × 10 in some cases); the resulting behavior of the energy roots is more complicated and difficult to understand. For qualitative understanding, it is probably best to begin with the states and energies of the linear model and to think of the additional off-diagonal terms of the nonlinear model as a perturbation on these. This perturbative mixing of states becomes large when a pair of linear states with the same S and S_{12} quantum numbers approach one another (i.e., for linear states differing only in S^*), and there is consequently a noncrossing rule for these states. These eigenstates will cross in the linear model but not in the nonlinear model. Further, there is a qualitative change in the nature of the lowest eigenstate as it passes through the region of near crossing in the nonlinear model, since there is strong mixing of basis states in this region. Conversely, if all interacting states with the same S and S_{12} values

(1) Noodleman, L. *Inorg. Chem.*, preceding paper in this issue.
(2) Carney, M. J.; Papaefthymiou, G. C.; Spartalian, K.; Frankel, R. B.; Holm, R. H. *J. Am. Chem. Soc.* **1988**, *110*, 6084.
(3) (a) Auric, P.; Gaillard, J.; Meyer, J.; Moulis, J. M. *Biochem. J.* **1987**, *242*, 525. (b) Gaillard, J.; Moulis, J. M.; Auric, P.; Meyer, J. *Biochemistry* **1986**, *25*, 464. (c) Moulis, J. M.; Auric, P.; Gaillard, J.; Meyer, J. *J. Biol. Chem.* **1984**, *259*, 11396.
(4) (a) Patil, D. S.; Moura, J. J. G.; He, S. H.; Teixeira, M.; Prickil, B. C.; DerVartanian, D. V.; Peck, H. D., Jr.; LeGall, J.; Huynh, B. H. *J. Biol. Chem.* **1988**, *263*, 18732. (b) Telser, J.; Benecky, M. J.; Adams, M. W. W.; Mortenson, L. E.; Hoffman, B. M. *J. Biol. Chem.* **1986**, *261*, 13536.

0020-1669/91/1330-0256$02.50/0

are far apart in some region of parameter space, then the linear model energies and properties will be close to those of the more exact nonlinear model there. Deviations of the nonlinear from the linear model are therefore largest near the linear model crossing points (between states having equal S and S_{12}), and it is just the behavior in this region of parameter space that is altered in such a way to provide a better representation of $S = {}^3/_2$ states and also for anomalous $S = {}^1/_2$ states found in *D. vulgaris* hydrogenase. By contrast, the properties of typical $S = {}^1/_2$ states of reduced ferredoxins are about equally well described by the nonlinear and linear models because the states are fairly similar, well away from an avoided crossing. (Still there are detailed differences in predicted properties between the linear and nonlinear models because there is always basis state mixing in the latter, and this mixing will vary with α and B/J_1.)

II. Generalized Hamiltonian Matrix

The Hamiltonian operator assumed is found in eq 5 of P 1 as before, but now the resonance electron transfer event is allowed to occur in a more general way. Before, electron transfer was assumed to couple only energetically degenerate states $|A(S,S_A^*,S_{12})\rangle$ and $|B(S,S_B^*,S_{12})\rangle$ so that the quantum number $S^* = S_A^* = S_B^*$ is preserved during the electron transfer. This is essentially an assumed selection rule for interaction between the Heisenberg basis states. This selection rule is only approximate since $-BT_{34} = -B(S_{34} + {}^1/_2)$ does link states for which $S_A^* \neq S_B^*$. As before, T_{34} is the electron-transfer operator for the subdimer containing sites 3 and 4. The importance of these off-diagonal matrix elements in S^* is governed by the size of the resonance matrix element, of course, but also by the closeness of approach of curves having common values of S and S_{12} but different values of S^* in the preceding linear model in P 1. There is a noncrossing rule for the intersection of these curves in the more general model. The previous matrices which are always of dimension 2×2 are replaced by larger matrices of row and column dimensions twice the number of allowed S^* values for specified S and S_{12}, and the diagonalization of these matrices yields the eigenstate vectors and eigenvalues of the problem. The variational principle holds so that the lowest state for each $|S\ S_{12}\rangle$ lies below the lowest $|S\ S^*\ S_{12}\rangle$ state of the linear model. The present model is nonlinear in the parameter α because there are a number of different Heisenberg energies E_{Heis} along the diagonal of the matrix in contrast to the previous model, which was linear in α.

Previously, we specified the eigenstates by the proper spin quantum numbers $|S\ S^*\ S_{12}\rangle$ and the localization by the coefficients c_A and c_B. In the more general problem $|S\ S_{12}\rangle$ remain as good quantum numbers because these are not mixed by resonance $-BT_{34}$ over the pair of sites 3 and 4; however, there is mixing of the spin quantum numbers S_A^* for $|A\rangle$ and S_B^* for $|B\rangle$. As before, we will suppress the S and S_{12} indices common to a vector and write

$$\Psi_G = \sum_{S_A^*} c_A(S_A^*)|A(S_A^*)\rangle + \sum_{S_B^*} c_B(S_B^*)|B(S_B^*)\rangle \quad (1a)$$

$$\Psi_G = N_A[\sum_{S_A^*} c_{AN}(S_A^*)|A(S_A^*)\rangle] + N_B[\sum_{S_B^*} c_{BN}(S_B^*) \times |B(S_B^*)\rangle] = N_A\Psi_A + N_B\Psi_B \quad (1b)$$

Equation 1b expresses the general state Ψ_G as a linear combination of the local normalized states Ψ_A and Ψ_B with normalized mixing coefficients N_A and N_B. The coefficients c_{AN} and c_{BN} are normalized over possible values of S_A^* and S_B^*, respectively. Equations 1a and 1b are entirely equivalent, but eq 1b is more convenient for the evaluation of hyperfine and EPR properties.

A separate matrix eigenvalue equation can be defined for each allowed value of S and S_{12}. The matrix is indexed by the allowed values for S_A^* and S_B^*; both have the same range and allowed values. For S_A^*, allowed values are determined by two inequalities:

$$|S - S_4| \leq S_A^* \leq S + S_4 \quad (2a)$$

and

$$|S_{12} - S_3| \leq S_A^* \leq S_{12} + S_3 \quad (2b)$$

where all site quantum numbers refer to states of type $|A\rangle$. The allowed values and ranges of S^* may be found by inspection of Table I in P 1; these are all S^* values allowed for given values of S and S_{12}. As before, the diagonal elements are the solutions of the Heisenberg Hamiltonian $E(S,S^*)$ (eq 2 of P 1), but there are a number of elements because of the variation in the quantum number S^*. The off-diagonal elements are the same as before for $S_A^* = S_B^*$, but new elements appear for $S_A^* \neq S_B^*$. Explicitly, these matrix elements are (valid for both $S_A^* = S_B^*$ and $S_A^* \neq S_B^*$) as follows:

$$-(E_{res})_{BA} = \langle B(S,S_B^*,S_{12})|H_{res}|A(S,S_A^*,S_{12})\rangle = -\sum_{S_{34}} B(S_{34} + {}^1/_2)U(S\ S_{34}\ S_A^*S_{12})U(S\ S_{34}\ S_B^*S_{12}) \quad (3)$$

where[5]

$$U(S\ S_{34}\ S_A^*S_{12}) = (-1)^{P_1}[(2S_A^* + 1)(2S_{34} + 1)]^{1/2}\begin{Bmatrix} S & S_{12} & S_{34} \\ S_3^A & S_4^A & S_A^* \end{Bmatrix} \quad (4)$$

$$U(S\ S_{34}\ S_B^*S_{12}) = (-1)^{P_2}[(2S_B^* + 1)(2S_{34} + 1)]^{1/2}\begin{Bmatrix} S & S_{12} & S_{34} \\ S_4^B & S_3^B & S_B^* \end{Bmatrix}$$

where $P_1 = S_{12} + S_3^A + S_4^A + S$ and $P_2 = S_{12} + S_4^B + S_3^B + S$ so that $(-1)^{P_1 + P_2} = 1$; hence, the phase factor $(-1)^{P_1 + P_2}$ does not affect the matrix element. The matrix E_{res} is symmetric; $(E_{res})_{BA} = (E_{res})_{AB}$. Assembling the c_A and c_B coefficients into vectors, we obtain the matrix eigenvalue equation:

$$\begin{bmatrix} (E_{Heis})_{AA} - E_{loc}/2 - E & -(E_{res})_{BA} \\ -(E_{res})_{AB} & (E_{Heis})_{BB} + E_{loc}/2 - E \end{bmatrix}\begin{bmatrix} \vec{c}_A \\ \vec{c}_B \end{bmatrix} = 0 \quad (5)$$

The eigenvalues and eigenvectors of this equation can be obtained by standard methods with the eigenstates and energies indexed as $|S\ S_{12}\ (r)\rangle$ and $E(S\ S_{12}\ (r))$, where r labels the roots of the equation. We will focus largely on the lowest roots for each S and S_{12}.

As in the preceding paper, I have written a set of computer codes to implement the appropriate algorithms, including both the energies and the hyperfine and EPR properties discussed next; the Racah coefficient subroutine used was written by J. P. Desclaux, and the matrix diagonalization subroutine was written by D. F. Mayers and J. P. Desclaux utilizing the QR method. Calculations were performed on a Convex C1 computer at Scripps, and plotting utilized a SUN 3/50 computer. These computer codes are available from the author.

III. Hyperfine and EPR Properties

For the evaluation of EPR and hyperfine properties, we begin with the same equations as in P 1 based on the Wigner–Eckart theorem.

$$A_i = a_i\frac{\langle S_{iz}\rangle}{\langle S_z\rangle} = K_i a_i \quad (6)$$

$$g_{eff} = \sum_i K_i g_i \quad (7)$$

In using equations based on the Wigner–Eckart (WE) theorem, we notice that K_i can be written either as a single quotient or a product of quotients. The denominators in these quotients must contain only good quantum numbers for the states according to the principles of WE.[5] As before, the hyperfine and EPR

(5) (a) Brink, D. M.; Satchler, G. R. *Angular Momentum*, 2nd ed.; Oxford University Press: London, 1968. (b) Edmonds, A. R. *Angular Momentum in Quantum Mechanics*; Princeton University Press: Princeton, NJ, 1957; Chapter 6, pp 90–108. (c) Wigner, E. P. *Group Theory*; Academic Press: New York, 1959; Chapter 24, pp 296–303. (d) Merzbacher, E. *Quantum Mechanics*, 2nd ed.; John Wiley and Sons: New York, 1970; Chapter 16, pp 396–404.

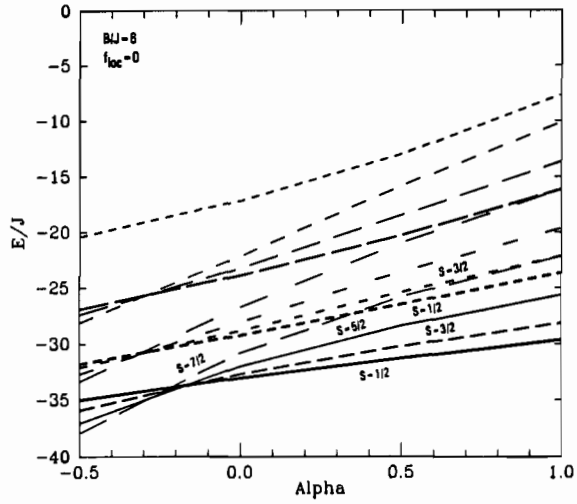

Figure 1. Energies of the low-lying spin states shown for $S = {}^1/_2, {}^3/_2, {}^5/_2$, and ${}^7/_2$ and $S_{12} = 4$. The nonlinear model was used with $B/J = 6$ and $f_{loc} = 0$ (delocalized states). The matrices are diagonalized for a discrete set of α points spaced at intervals of $\Delta\alpha = 0.25$ and linearly interpolated to give the curves.

properties can be evaluated separately for the local states Ψ_A and Ψ_B and then weighted by N_A^2 and N_B^2, respectively. Again, it is sufficient to consider the properties of Ψ_A; those of Ψ_B can be evaluated by analogous procedures. For the state Ψ_A, the site spin quantum numbers are $S_1 = S_2 = S_3 = 2$ and $S_4 = {}^5/_2$, while for Ψ_B the spin quantum numbers of sites S_3 and S_4 are permuted; further, $S_{124}{}^B = S_B{}^*$ plays a role for Ψ_B entirely analogous to $S_{123}{}^A = S_A{}^*$ for Ψ_A. Because S^* is no longer a good quantum number for Ψ_A or Ψ_B, we reconstruct the quotients so that only quantum numbers S and S_{12} appear in the denominator.

The following relationship still holds:

$$K_i = \frac{\langle S_{iz}\rangle}{\langle S_z\rangle} = \frac{\langle \vec{S}\cdot\vec{S}_i\rangle}{S(S+1)} \tag{8}$$

where the expectation value is taken over Ψ_A. Using the modified form of eq 23 in P 1, we find

$$K_4 = \frac{\langle S_{4z}\rangle}{\langle S_z\rangle} = \frac{\langle \vec{S}\cdot\vec{S}_4\rangle}{S(S+1)} = \frac{[S(S+1) + S_4(S_4+1) - \langle \vec{S}_{123}{}^2\rangle]}{2S(S+1)} \tag{9}$$

Evaluating K_1 and K_2

$$K_1 = K_2 = \frac{\langle S_{1z}\rangle}{\langle S_{12z}\rangle}\cdot\frac{\langle S_{12z}\rangle}{\langle S_z\rangle} = \frac{\langle \vec{S}_1\cdot\vec{S}_{12}\rangle}{S_{12}(S_{12}+1)}\cdot\frac{\langle \vec{S}_{12}\cdot\vec{S}\rangle}{S(S+1)} = \frac{[S(S+1) + S_{12}(S_{12}+1) - \langle \vec{S}_{34}\cdot\vec{S}_{34}\rangle]}{4S(S+1)} \tag{10}$$

As previously shown in P 1 (eqs 25 and 26), $K_3 = 1 - K_1 - K_2 - K_4$. In evaluating these matrix elements, we can represent Ψ_A as a linear combination of kets $|A(S_A{}^*)\rangle$ (eq 1b) for matrix elements of $\langle \vec{S}_{123}{}^2\rangle$ and for other terms of the form $\langle \vec{S}_{34}\cdot\vec{S}_{34}\rangle$ we must expand these kets as linear combinations of $|(S_{12})(S_{34}{}^A)S\rangle$ precisely as in eq 6 of P 1.

It is important to notice that because of terms of the type $\langle \vec{S}_{34}\cdot\vec{S}_{34}\rangle$, the properties of the nonlinear eigenstates are not simply weighted averages of the properties of the basis states $|A(S_A{}^*)\rangle$, since there are also cross-terms among these.

IV. Results: Energies and Properties

A. Energy Diagrams. In Figures 1–5, a number of the low-lying spin states of the model are plotted for $B/J = 6$, 4, 3, and 2.5. (For simplicity, J refers to J_1.) At $B/J = 6$, both the delocalized states and the partially localized states are shown at $f_{loc} = 0$ and $f_{loc} = 5$, respectively, in Figures 1 and 2. In all cases, we have displayed only states with $S_{12} = 4$, since these are the lowest over the appropriate range in parameter space. These figures show

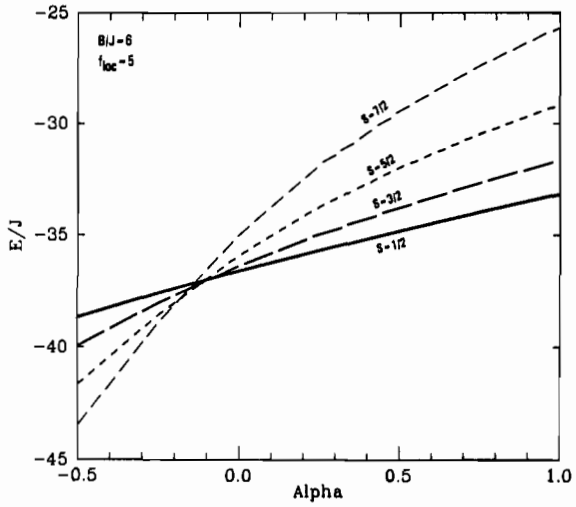

Figure 2. For $B/J = 6$ and $f_{loc} = 5$ (partially localized), plots of the lowest energy state for each spin $S = {}^1/_2, {}^3/_2, {}^5/_2$, and ${}^7/_2$ and with $S_{12} = 4$.

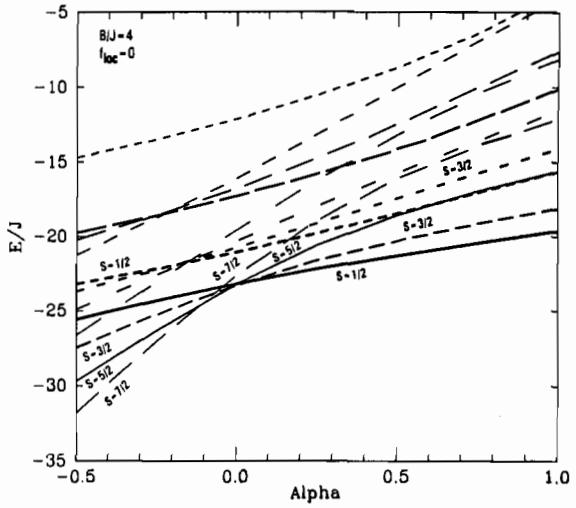

Figure 3. For $B/J = 4$ and $f_{loc} = 0$, plots of the energies of low-lying spin states. The states shown are the same as for Figure 1.

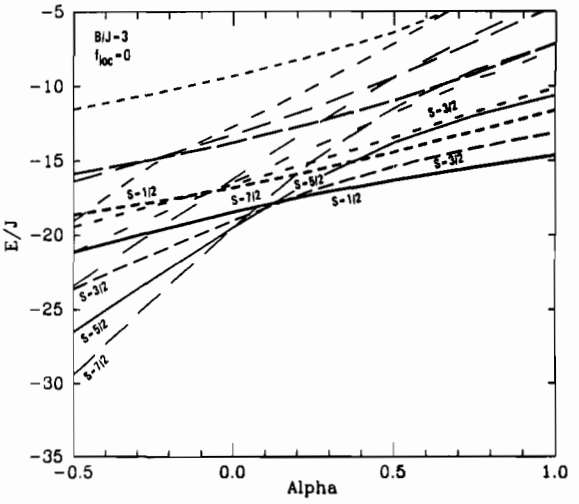

Figure 4. For $B/J = 3$ and $f_{loc} = 0$, plots of the energies of low-lying spin states. The states shown are the same as for Figure 1.

that over most of the range of α and B/J, $S = {}^3/_2$ is in much closer proximity to $S = {}^1/_2$ than in the linear model, comparing Figures 1, 2, and 4 with Figure 4a–c of P 1. There is also a larger region in parameter space where $S = {}^3/_2$ is the ground state or at least where $S = {}^1/_2, {}^3/_2, {}^5/_2$, and ${}^7/_2$ possess nearly coexisting ground states. Compared to the linear model, the nonlinear model has

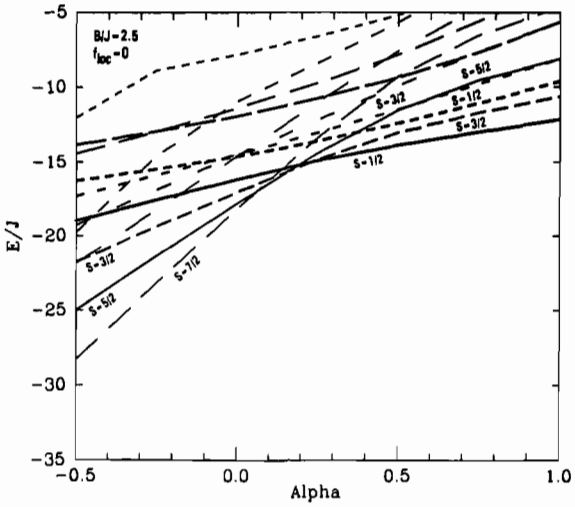

Figure 5. For $B/J = 2.5$ and $f_{loc} = 0$, the energies of low-lying spin states. The states are the same as for Figure 1.

crossing points at more positive α, and these crossing points between the lowest states of different total spin shift to more positive α with decreasing B/J. (The latter trend is seen in the linear model as well.) The region of stability of $S = {}^1/_2$ varies with B/J so that $\alpha \geq -0.1$ at $B/J = 6$, $\alpha \geq +0.05$ at $B/J = 4$, and $\alpha \geq +0.18$ at $B/J = 3$; at these boundaries, $S = {}^3/_2$ crosses below $S = {}^1/_2$.

There is also a strong contrast between the avoided crossings displayed by the nonlinear model between states having the same values of S and S_{12} and crossings of the analogous curves in the linear model; Figures 1, 2, and 4 can be compared directly with Figure 4a–c of P 1. As expected, we have calculated strong basis state mixing in the vicinity of the avoided crossings.

B. EPR and Hyperfine Properties for $S = {}^1/_2$. From the perspective of EPR and hyperfine properties, the most important feature of the nonlinear model is the variability of g_{av} and A_{av} continuously as a function of B/J and α in contrast to the constant values (see Table IV of P 1) given by the linear model for each particular spin-state eigenvector. In the nonlinear model, the spin eigenvectors vary continuously with the parameters B/J and α; no such variation occurs in the linear model. (The properties in both the linear and nonlinear models vary with the localization parameter f_{loc}.)

We will consider first the predicted properties of the lowest $S = {}^1/_2$ state over the region in parameter space where this is the ground state. Parts a–d of Figure 6 show the predicted g_{av} values and parts a–d of Figure 7 the predicted effective A_{av} values for delocalized $S = {}^1/_2$ states at $B/J = 6, 4, 3, 2.5$. We have used the same intrinsic site parameters as in P 1; specifically, $\Delta g(Fe^{2+}) = 0.05$, $a(Fe^{2+}) = -22$ MHz, and $a(Fe^{3+}) = -20$ MHz. For typical reduced 4Fe ferredoxins with $S = {}^1/_2$ ground states, observed effective A_{av} are around −30 MHz for Fe^{3+}–Fe^{2+} and about 16 MHz for Fe^{2+}–Fe^{2+} from Mossbauer spectroscopy; the cor-

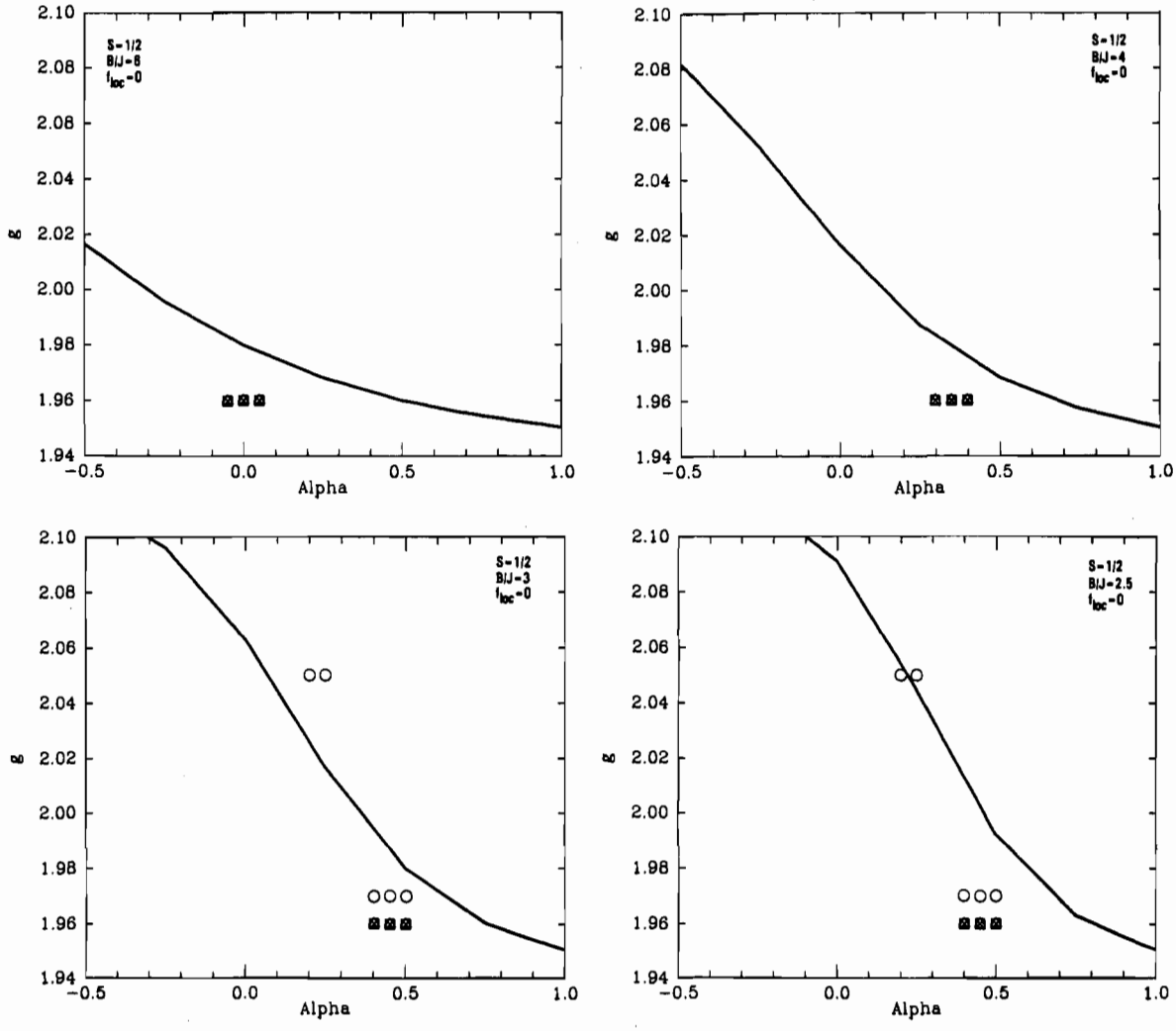

Figure 6. Predicted theoretical g_{av} values (solid line) versus α for the lowest $S = {}^1/_2$ state having $S_{12} = 4$. $B/J = 6, 4, 3$, and 2.5 for (a, top left)–(d, bottom right), respectively. Experimental points are for $Fe_4S_4(S\text{-}p\text{-}C_6H_4Br)_4^{3-}$, *B. stearothermophilus* Fd., and Av2 protein in ethylene glycol for triangles, squares, and crosses, respectively. In (c, bottom left) and (d, bottom right), the g_{av} values at 1.97 and 2.05 characteristic of the rhombic "2.06" and "2.10" signals from the special cluster (cluster no. 3) in *D. vulgaris* hydrogenase are depicted by circles. The positions of the experimental points with respect to α (horizontally) were determined by optimizing simultaneously both g_{av} and A_{av} from the experiments to the various theoretical curves subject to the constraint that $S = {}^1/_2$ is the ground state only over a limited region in parameter space.

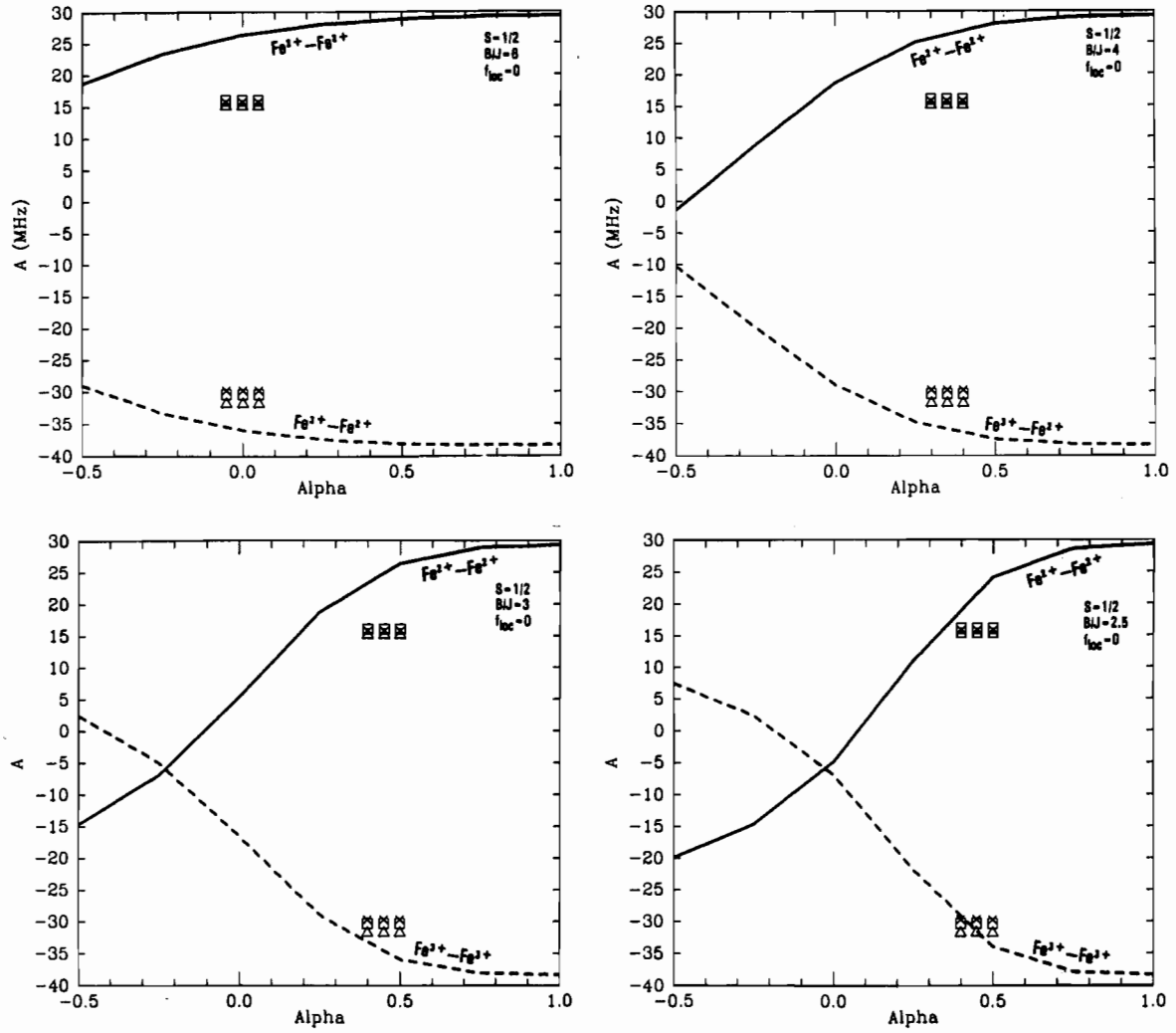

Figure 7. Predicted theoretical A_{av} values for the lowest state with $S = {}^1/_2$ and $S_{12} = 4$. $B/J = 6$, 4, 3, and 2.5 for (a, top left)–(d, bottom right), respectively. Experimental points correspond to those for the clusters in Figure 6. The solid lines (theory) and positive experimental points are for the Fe^{2+}–Fe^{2+} pair with the dashed lines (theory) and negative experimental points for the Fe^{3+}–Fe^{2+} delocalized pair.

responding g_{av} is typically 1.96 (Table IV of P 1).[2,3,6,7]

When comparing predicted and experimental g_{av} and A_{av} values, we have the freedom to translate the experimental values horizontally to achieve an optimal fit, since the correct value of α is a prior unknown. For the $S = {}^1/_2$ state, this is subject to the constraint that $S = {}^1/_2$ is the ground state only over a limited region in parameter space as specified above. By simultaneously finding an optimal range of α for both g_{av} and A_{av}, we obtain differing α ranges as a function of B/J, as shown in Figures 6 and 7. For typical reduced ferredoxins with $S = {}^1/_2$ ground states, there is no uniquely optimal value of B/J and α. Instead, the range from $6 \geq B/J \geq 2.5$ appears acceptable; there is always some error in the fit when both g and A are optimized. The general level of agreement between theory and experiment is similar to that displayed by the linear model.

In aconitase, the reduced substrate bound form has larger hyperfine $|A_{av}|$ values than typical reduced ferredoxins;[8] the signs of these correspond to the expected spin-coupling pattern for the observed $S = {}^1/_2$ ground state. Partial results are also available for the substrate-free form based on ENDOR data. Because the local coordination is different for one Fe site in aconitase both in the substrate-free and substrate-bound forms, the differences observed in A and g values are not surprising. We will defer any detailed consideration of this problem. For further information, there is a good review of recent spectroscopic studies on aconitase by Beinert and Kennedy.[8]

C. Properties of *D. vulgaris* Hydrogenase. The protein *D. vulgaris* hydrogenase possesses three 4Fe–4S clusters from the studies of Huynh et al.[4] Two of these display EPR spectra similar to those of typical reduced 4Fe ferredoxins, while the third cluster in the reduced form has two rhombic EPR signals under different conditions. These are called the rhombic "2.06" signal and the rhombic "2.10" signal from their maximum principal g values. The corresponding g_{av} values are 1.97 and 2.05, respectively. On the basis of its redox behavior, Huynh et al.[4] have proposed that these two states represent two different conformations in the same +1 cluster oxidation state. We have included the g_{av} values from the two rhombic states of *D. vulgaris* hydrogenase (open circles) in Figure 6c,d corresponding to $B/J = 3$ and 2.5. At this low B/J ratio, the strong variability in g displayed by the two rhombic states can be reproduced with a modest variation in α between about 0.5 and 0.2 for the lower and higher g_{av} values. The presence of two widely differing EPR signals cannot be explained by larger B/J values ($B/J > 4$), since there is insufficient variability in the allowed region of parameter space. Further, Huynh[9] has observed that the larger g value is associated with A_{av} having smaller magnitudes from Mossbauer spectroscopy. This is just the trend shown in Figure 7c,d. Accurate measurements of the physical properties for this cluster are continuing in Huynh's laboratory,[9] which will allow further detailed comparisons with our theoretical model.

(6) Lindahl, P. A.; Day, E. P.; Kent, T. A.; Orme-Johnson, W. H.; Munck, E. *J. Biol. Chem.* **1985**, *260*, 11160.
(7) Middleton, P.; Dickson, D. P. E.; Johnson, C. E.; Rush, J. D. *Eur. J. Biochem.* **1978**, *88*, 135.
(8) Beinert, H.; Kennedy, M. C. *Eur. J. Biochem.* **1989**, *186*, 5.
(9) Huynh, B. H. Personal communication.

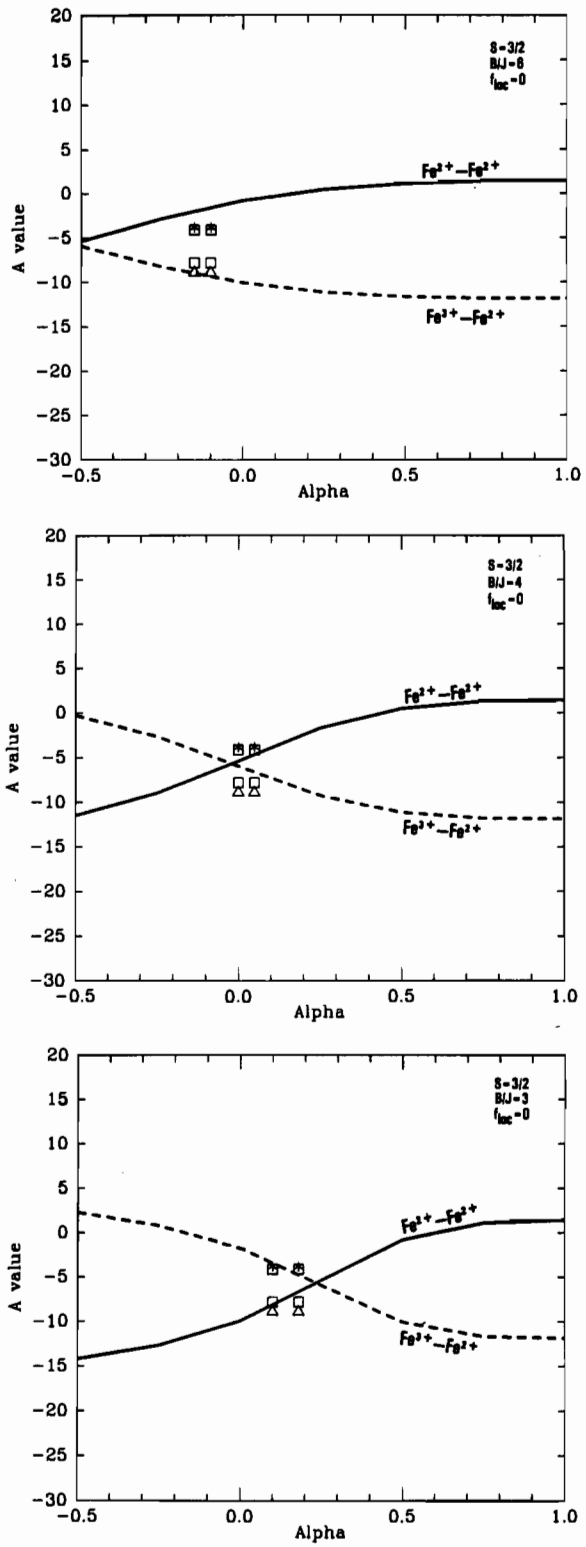

Figure 8. Predicted A_{av} values for the lowest $S = {}^3/_2$ state with $S_{12} = 4$ compared to experimental results for the Av2 protein in urea solution (squares), the synthetic complex $Fe_4S_4(SR)_4^{3-}$, where R = C_6H_{11} (triangles), and Se Cp ferredoxin (asterisks). The upper solid line is for the Fe^{2+}–Fe^{2+} pair and the lower dashed line is for the Fe^{3+}–Fe^{2+} pair. The parameter values $B/J = 6$, 4, and 3 and $f_{loc} = 0$ give good agreement with the experimental points. Further, the horizontal positions of the experimental points were chosen to correspond to the small region in parameter space where $S = {}^3/_2$ is the ground state or where the lowest $S = {}^1/_2$, ${}^3/_2$, and ${}^5/_2$ states are nearly coexisting ground states.

D. Properties of $S = {}^3/_2$ States. In Figure 8, we display the predicted A values with the parameters $B/J = 6$, 4, and 3 and $f_{loc} = 0$ (delocalized) for the lowest $S = {}^3/_2$ state compared with observed hyperfine A values for three clusters with $S = {}^3/_2$ ground states from Av2 protein in urea solution (squares),[6] a synthetic complex (triangles) $Fe_4S_4(SR)_4^{3-}$, where R = C_6H_{11},[2] and from Se-substituted *Clostridium pasteurianum* (Se Cp) ferredoxin.[3] The experimental values are uniformly small and negative, and there is a good fit to the theoretical predictions. Again the horizontal position of the experimental values is determined by the position in parameter space where $S = {}^3/_2$ crosses below $S = {}^1/_2$ and also remains below $S = {}^5/_2$ and ${}^7/_2$. These levels are so close that they are nearly coexisting states over a small region in parameter space (Figures 1–5). Such a near coexistence is reasonable experimentally in the case of Av2, since variation of the composition of the solvent from 50% ethylene glycol to 0.4 M urea drastically changes the spin-state mixture from predominantly $S = {}^1/_2$ to predominantly $S = {}^3/_2$. In the case of Se Cp ferredoxin, there are coexisting $S = {}^1/_2$, ${}^3/_2$, and ${}^7/_2$ ground states.

Experimentally, it is very difficult to determine the small hyperfine parameters of these $S = {}^3/_2$ states accurately by Mossbauer spectroscopy.[3,6,10] While the theory at $B/J = 6$ indicates that the more negative A value is associated with the mixed-valence Fe^{3+}–Fe^{2+} pair and the less negative with the Fe^{2+}–Fe^{2+} pair, this correspondence is unclear on the basis of the Mossbauer spectroscopy of Av2/urea;[6,10] further, the quantitative accuracy of the A values is not high. Overall, however, the experiments indicate site equivalence in pairs and rather isotropic hyperfine coupling. For the synthetic cluster,[2] only a single type of site was found from the collected results of Mossbauer isomer shifts, quadrupole splittings, and hyperfine couplings (A values). The experimental A values are anisotropic, and an average of these was used to compare with the theory. (Note also that the magnetic hyperfine parameters from ref 2 were converted to refer to the ground state of the ^{57}Fe nucleus rather than the excited state.) For Se Cp ferredoxin,[3] a small negative isotopic hyperfine tensor was found; only one type of site was resolved, but the broad lines seen by Mossbauer spectroscopy may indicate some inequivalence among iron sites. An equally good fit to the experimental results for these three clusters is attained for $B/J = 4$ and 3. For the value $B/J = 3$, the assignment of the mixed-valence and ferrous pairs is reversed with respect to that for $B/J = 6$ and 4. We conclude that B/J values in the entire range $6 \geq B/J \geq 3$ provide an acceptable fit to the available experimental hyperfine for $S = {}^3/_2$ states.

For the nonlinear model to provide a good fit to negative hyperfine constants found for various $S = {}^3/_2$ states, it is necessary that there be strong mixing among the basis vectors $|S\ S^*\ S_{12}\rangle = |{}^3/_2\ 2\ 4\rangle$, $|{}^3/_2\ 3\ 4\rangle$, and $|{}^3/_2\ 4\ 4\rangle$ in the lowest eigenstate $|S\ S_{12}\ (r)\rangle = |{}^3/_2\ 4\ (1)\rangle$. We have found this from the calculations. Because of the requirements that the energy state be the lowest overall and that the predicted hyperfine A_{av} values be close to those observed experimentally, none of the $S = {}^3/_2$ states from the linear model is acceptable (see Table V of P 1). The interaction of the various $S = {}^3/_2$ basis states leads to a significant lowering of the lowest $S = {}^3/_2$ eigenstate in accordance with the variational principle. This lowering is larger than that exhibited by the lowest $S = {}^1/_2$ eigenstate by a similar mechanism (mixing of the two possible $S = {}^1/_2$ basis vectors $|{}^1/_2\ 2\ 4\rangle$ and $|{}^1/_2\ 3\ 4\rangle$), and this has a significant effect on the $S = {}^1/_2$ to $S = {}^3/_2$ state crossing as well as on predicted properties.

E. Properties of the $S = {}^7/_2$ State in Reduced Se Ferredoxin. In Figure 9, we compare the predicted theoretical A_{av} values for the lowest $S = {}^7/_2$ state with the observed hyperfine properties for the $S = {}^7/_2$ state of Se-substituted Cp ferredoxin. We have chosen a partially localized ($f_{loc} = 5$) situation and $B/J = 6$ and 4, both of which provide a good fit to experiment for a selected range of α where $S = {}^7/_2$ is the system ground state. As noted previously in P 1 (Table VII), either partial or complete localization is required to obtain a 3:1 site equivalence ratio of localized Fe^{2+} to Fe^{3+} sites. The predictions of the nonlinear model like those of the simpler linear model are quite good for the observed localized $S = {}^7/_2$ state. Our calculations support the validity of the empirical spin-coupling model of Gaillard et al.[3] and dem-

(10) Munck, E. Personal communication.

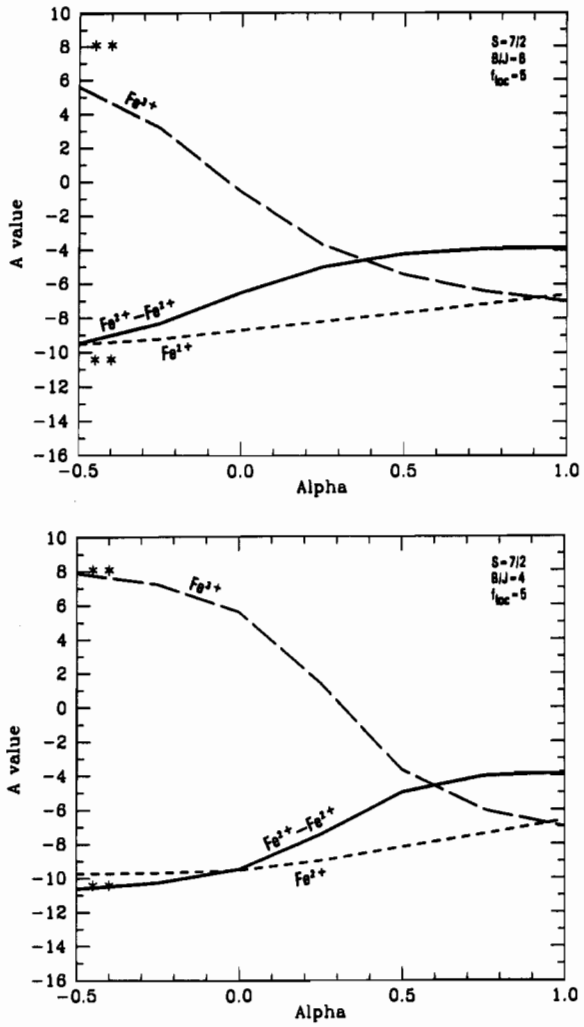

Figure 9. Predicted A_{av} values for the lowest $S = {}^7/_2$ state with $S_{12} = 4$ at (a, top) $B/J = 6$ and $f_{loc} = 5$ (partially localized) and (b, bottom) $B/J = 4$ and $f_{loc} = 5$. There are three theoretical curves for the Fe^{2+}–Fe^{2+} S_{12} pair (solid line), for a distinct Fe^{2+} site derived from localization of the mixed-valence pair (short dashed line), and for the Fe^{3+} site also derived from localization of the mixed-valence pair (long dashed line). The horizontal location of the data points is chosen to give a good fit of theory to experiment and lies in the region where $S = {}^7/_2$ is the cluster ground state. Experimental values are from the $S = {}^7/_2$ state of Se Cp ferredoxin (asterisks).

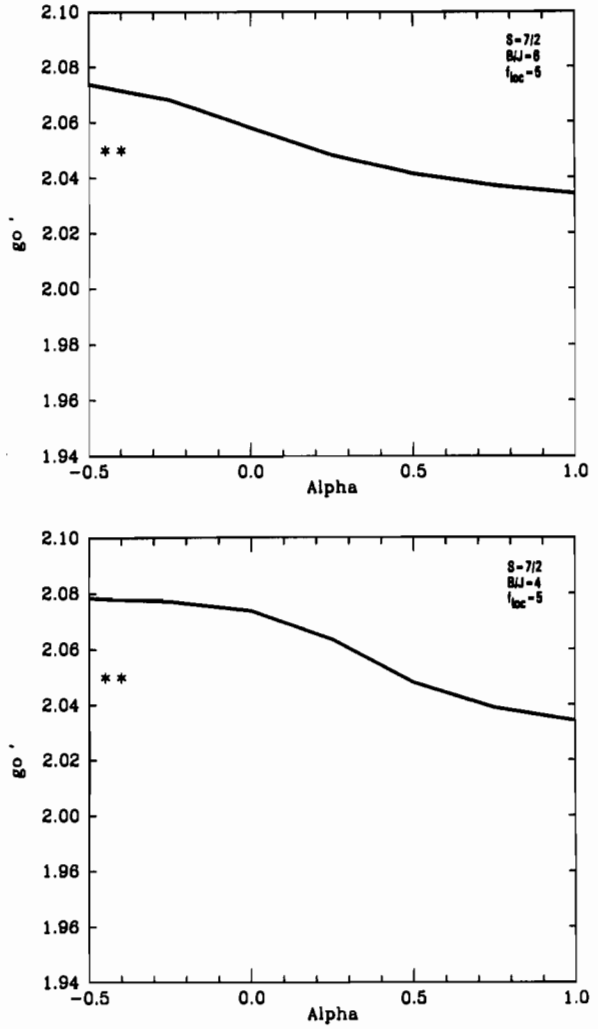

Figure 10. Predicted (g_0') values (solid line) for the lowest $S = {}^7/_2$ state with $S_{12} = 4$ at (a, top) $B/J = 6$ and $f_{loc} = 5$ and (b, bottom) $B/J = 4$ and $f_{loc} = 5$. Experimental values (asterisks) are from best fits of the EPR spectra of Se Cp ferredoxin to a Zeeman plus zero-field-splitting Hamiltonian, quoted as $g_0 = 2.05$ in Gaillard et al.

onstrate how a state of this type can be strongly stabilized.

F. Zero-Field-Splitting Effects. An effective spin Hamiltonian for describing the electronic states of spin systems with $S > {}^1/_2$ is[3,11]

$$H^s = H_1^s + H_2^s = \beta\vec{B}\cdot g_0'\cdot\vec{S} + D[S_z^2 - {}^1/_3 S(S+1)] + E[S_x^2 - S_y^2] \quad (11)$$

expressed as a sum of a Zeeman term (H_1^S) and two zero-field-splitting terms (H_2^s), omitting hyperfine and other electron–nuclear interactions. This spin Hamiltonian acts on the various components $|S\ M_s\rangle$ of the state with total spin S. The observed effective g values are often highly anisotropic for the various Kramers doublets, and to calculate these we need to diagonalize the Hamiltonian matrix involving all the parameters g_0', D, and E. The values of these parameters can then be obtained empirically from fits to the EPR spectra as a function of temperature, with additional information from the shape and temperature dependence of the magnetic Mossbauer spectra.[3] (Each Kramers doublet is considered as a pseudospin $S' = {}^1/_2$ system for analysis of the EPR spectra at X-band.) Obtaining all the parameters theoretically is difficult. However, the parameter g_0' in the Zeeman term of this Hamiltonian should be given simply by the Wigner–Eckart theorem for vector operators as previously developed. This follows from the fact that both the Zeeman and zero-field-splitting terms are obtained as a consequence of second-order perturbation theory[12] and the Wigner–Eckart theorem should apply to each separately so long as there is no significant mixing of different total S states.[13] (When mixing of different S states is present, the most general form of the Wigner–Eckart theorem is still applicable, but this leads to expressions that are considerably more involved.[13]) Assuming that g_0' is isotropic, the nonlinear theory gives a reasonably good match to the value of g_0' determined empirically for the $S = {}^7/_2$ state of Se Cp ferredoxin ($g_0' = 2.05$),[3] as shown in Figure 10. The predicted values are 2.07–2.08.

The zero-field-splitting parameters should be susceptible to a similar treatment. However, since the zero-field-splitting terms constitute a second-rank tensor,[13] applying the Wigner–Eckart theorem to derive a relationship between the D and E parameters for total S and the corresponding intrinsic parameters for the site spins S_i is rather complicated and will not be pursued here.

G. Special Cases. As the algorithms for the spin-state energies and properties in this paper are rather complex, it is useful to have

(11) Abragam, A.; Bleaney, B. *Electron Paramagnetic Resonance of Transition Ions*; Dover: New York, 1986.

(12) McWeeney, R.; Sutcliffe, B. T. *Methods of Molecular Quantum Mechanics*; Academic Press: New York, 1976; Chapter 8, pp 210–233.

(13) Scaringe, R. P.; Hodgson, D. J.; Hatfield, W. E. *Mol. Phys.* **1978**, *35*, 701.

some simple checks on the correctness of the results in limiting cases. A good check is provided by the point $\alpha = 1$ where $J_1 = J_2$. Since all J parameters are the same, the solution to the Heisenberg exchange and resonance Hamiltonian at this point is[14,15]

$$E(S,S_{34}) = (J/2)[S(S+1)] \pm B(S_{34} + {}^1/_2) \qquad (12)$$

The eigenstates of this can be specified as $|S\ S_{12}\ S_{34}\rangle$, and there is often degeneracy in S_{12} consistent with the triangle inequality. The consequences of eq 12 and the use of the triangle inequality for the eigenstates $|S\ S_{12}\ S_{34}\rangle$ have been analyzed in our previous paper on $[Fe_4S_4]^{3+}$ clusters.[14] The triangle inequality is

$$(S + S_{34}) \geq S_{12} \geq |S - S_{34}| \qquad (13)$$

In addition, S_{12} is subject to the restriction that $S_{12} \leq |S_1 + S_2|$. Also, from the Wigner–Eckart theorem, closed-form solutions can be given for K_1, K_2, K_3, and K_4, which allows direct computation of A and g values.[14] The relevant equations for the point $\alpha = 1$ are the same as in ref 14; however, for $[Fe_4S_4]^{1+}$ clusters, $S_1 = S_2 = 2$ in place of $S_1 = S_2 = {}^5/_2$ for $[Fe_4S_4]^{3+}$ clusters. (Note that, for the simple exchange and resonance Hamiltonian assumed in ref 14, $|S\ S_{12}\ S_{34}\rangle$ are always eigenstates of the system, even with unequal J parameters. For the more sophisticated Hamiltonian assumed in the present work, $|S\ S_{12}\ S_{34}\rangle$ are proper eigenstates only at $\alpha = 1$.)

A few examples will make these ideas more concrete. At $\alpha = 1$, the lowest lying $S = {}^1/_2$ state has quantum numbers $|S\ S_{12}\ S_{34}\rangle = |{}^1/_2\ 4\ {}^9/_2\rangle$, giving $K_1 = K_2 = -1.333$, $K_3 = 2.037$ (for Fe^{3+}), and $K_4 = 1.630$ (for Fe^{2+}), using the equations in ref 14; this corresponds to the local state $|B\rangle$. The resulting $g_{eff} = 1.950$, which coincides exactly with the g_{eff} predicted by using eqs 6–10 of the present work at $\alpha = 1$ (Figure 6). Further, g_{eff} at $\alpha = 1$ is independent of B/J, as shown in Figure 6, and required theoretically. The predicted A_{av} values are +29.333 MHz for the ferrous pair and −38.296 MHz for the delocalized Fe^{3+}–Fe^{2+} pair, using the K_i values above. Again, this precisely corresponds to the values computed by using eqs 6–10 of the present work in the limit $\alpha = 1$, and these values are independent of B/J (Figure 7). (All of these results for properties employ the same intrinsic site parameters previously defined.) We have also checked that the degeneracy of various $S = {}^3/_2$ and $S = {}^5/_2$ states is correct at the point $\alpha = 1$; for example, when $S = {}^3/_2$ and $S_{34} = {}^9/_2$, then $S_{12} = 3$ and 4 are degenerate at $\alpha = 1$. Also, at $\alpha = 1$, the delocalized state $|S\ S_{12}\ S_{34}\rangle = |{}^3/_2\ 4\ {}^9/_2\rangle$ has hyperfine parameters of +1.467 MHz and −11.837 MHz for the ferrous and mixed valence pairs, which are precisely the values determined in this limit by the nonlinear model for $|S\ S_{12}\ (r)\rangle = |{}^3/_2\ 4\ (1)\rangle$ (see Figure 8). The validity of the general equations and the computer algorithms in this limit provides strong support for the correctness of the nonlinear model. It is the proper model for the spin-state energies and properties given the physical assumptions of the combined Heisenberg plus resonance Hamiltonian. By contrast, the linear model does not give the correct limiting values at $\alpha = 1$, as shown by the g and A values in Tables IV and V of P 1.

V. Conclusions

The nonlinear model provides a good description of the properties of a variety of states having $S = {}^1/_2$, ${}^3/_2$, and ${}^7/_2$ in reduced $[Fe_4S_4]$ and $[Fe_4Se_4]$ clusters. We find that the lowest $S = {}^3/_2$ state energy is in much closer proximity to $S = {}^1/_2$ over an extended range of α than occurred with the linear model. This is consistent with the prevalence of statistical mixtures of $S = {}^1/_2$ and ${}^3/_2$ often found in these clusters. The close proximity of $S = {}^1/_2$ and ${}^3/_2$ states can also lead to spin-admixed systems when $S = {}^1/_2$ and ${}^3/_2$ mix through spin–orbit coupling. The close crossings exhibited by $S = {}^1/_2$, ${}^3/_2$, ${}^5/_2$, and ${}^7/_2$ in the model are also reasonable when compared with the coexisting ${}^1/_2$, ${}^3/_2$, and ${}^7/_2$ states found in $[Fe_4Se_4]$ proteins.

Reasonable predictions for average g and A values of $S = {}^1/_2$ states in typical 4Fe ferredoxins are found for parameters in the range $2.5 \leq B/J_1 \leq 6$ and $-0.1 \leq \alpha \leq 0.5$. The model shows how the large variation in average g values, 1.97 and 2.05, observed for the two different rhombic states of the unusual cluster in *D. vulgaris* hydrogenase can be closely represented by a modest variation in the α parameter, $0.2 \leq \alpha \leq 0.5$, at low B/J_1, $2.5 \leq B/J_1 \leq 3$. In contrast to the situation for typical ferredoxin clusters, only low values of B/J_1 provide an acceptable fit. Further, the smaller α value is associated with the larger g_{av} value. The predicted A_{av} values are much smaller in magnitude for $g_{av} = 2.05$ than for $g_{av} = 1.97$ (for EPR rhombic "2.10" versus rhombic "2.06" signals, respectively), a result that is in agreement with Mossbauer studies on this cluster.[9]

This variability cannot be properly represented by the linear model in P 1, as shown by Table IV. For low B/J_1 between 2 and 4, there will be a crossing point from ground-state $|S\ S^*\ S_{12}\rangle = |{}^1/_2\ 2\ 4\rangle$ to state $|{}^1/_2\ 3\ 4\rangle$ with decreasing α; the predicted associated change in g_{av} is from 1.94 to 2.14, which is far greater than the observed change. Also, both states have hyperfine A_{av} values of similar magnitude but differing signs for the various sites, predictions that conflict with the Mossbauer results.[9]

We find a good theoretical prediction of the small negative hyperfine constants on all Fe sites observed for various reduced ferredoxins in the $S = {}^3/_2$ ground state or where this state coexists with $S = {}^1/_2$ and ${}^7/_2$. Only a small region of parameter space with respect to α is allowed because of the behavior of the spin-state crossings; a larger B/J range is acceptable from $3 \leq B/J \leq 6$. The linear model does not give an acceptable representation of this behavior on the basis of Table V of P 1 (see also the discussion in this paper).

Theoretical A_{av} values for the Fe^{2+} and Fe^{3+} sites of the $S = {}^7/_2$ state are in good agreement with the observed values including the site ratio of 3:1 from Mossbauer spectroscopy in Se-substituted Cp ferredoxin. On the basis of these results, there must be at least partial localization of the mixed-valence pair by extrinsic forces, which may include hydrogen bonding or electrostatic effects of the protein polypeptide chain. The Zeeman parameter g_0' is also calculated with reasonable accuracy by the model compared with the value determined by EPR[3] spectroscopy.

Additional types of measurements will prove very important for testing the present nonlinear model more rigorously and for restricting the location of experimentally observed states to a smaller region in parameter space. These would include magnetic susceptibility measurements, as well as temperature-dependent EPR and Mossbauer experiments to determine the presence and character of low-lying spin states. Optical measurements can potentially provide a direct measurement of B, although the relevant frequencies will be in the infrared region. The relevant dipole and spin-allowed optical excitation will be polarized along the Fe–Fe axis of the delocalized mixed-valence pair because of the $\sigma \rightarrow \sigma^*$ Fe–Fe bonding to antibonding character of this transition. The energy of the transition is $2B\langle S_{34} + {}^1/_2\rangle$ for a delocalized electron, which is typically $8B$–$10B$ (for spin states with total $S = {}^1/_2$ and ${}^3/_2$ and with $\langle S_{34}\rangle$ between ${}^7/_2$ and ${}^9/_2$). The mixed-valence pair is Robin–Day class III.[16]

In the presence of external localizing forces (E_{loc}) or vibronic distortions, valence trapping is possible (Robin–Day class II), as in the $S = {}^7/_2$ ground state. This is a well-known vibronic problem with a double-well (either symmetric or nonsymmetric) lower surface for each spin state and a single-well upper surface.[17] The relevant optical transition is that of the intervalence charge-transfer band (E_{op}); this can be either in the infrared or the optical region of the spectrum depending on the strength of vibronic or other

(14) Noodleman, L. *Inorg. Chem.* **1988**, *27*, 3677.
(15) (a) Munck, E.; Papaefthymiou, V.; Surerus, K. K.; Girerd, J. J. In *Metals in Proteins*; ACS Symposium Series; Que, L., Ed.; American Chemical Society: Washington, DC, 1988; Chapter 15, pp 302–325. (b) Papaefthymiou, V.; Girerd, J. J.; Moura, I.; Moura, J. J. G.; Munck, E. *J. Am. Chem. Soc.* **1987**, *109*, 4703.
(16) Robin, M. B.; Day, P. *Adv. Inorg. Chem. Radiochem.* **1967**, *10*, 247.
(17) (a) Wong, K. Y.; Shatz, P. N. *Prog. Inorg. Chem.* **1981**, *28*, 369. (b) Koppel, H.; Cederbaum, L. S.; Domcke, W.; Shaik, S. S. *Angew. Chem., Int. Ed. Engl.* **1983**, *22*, 210.

localizing environmental forces. The intensity of such a band as a function of the dimer (or subdimer) spin state and temperature has been evaluated by Cox,[18] and similar equations should apply to tetramers having one or more mixed-valence pairs. Either vibronic tunneling or thermal hopping is possible on the lower double-well surface with barrier height E_ϕ. Expressions for E_{op}, E_ϕ, and the transition intensity have been given by Girerd[19] for spin-coupled dimers; again similar expressions should be applicable for tetramers, utilizing the subdimer spin quantum number $\langle S_{34} \rangle$. (Note, however, that the transition moment expressions may be oversimplified, since they are based on Huckel type equations.)

A brief summary of some remaining issues is appropriate. The detailed understanding of the presence and properties of "spin-admixed" states (often found in synthetic clusters), while generally consistent with the energy level scheme indicated by the nonlinear model, requires a closer analysis of the way spin-orbit coupling (zero-field splitting) will mix states of different total spin. The presence of an unusual $S = {}^5/_2$ or ${}^7/_2$ state as the ground state in oxidized P clusters of nitrogenase is not explained by the present model; rather, the $S = {}^7/_2$ state found by the model behaves like the observed $S = {}^7/_2$ in Se Cp ferredoxin. The lowest lying $S = {}^5/_2$ state has similar predicted properties. If the oxidized P clusters are in fact $[Fe_4S_4]$ clusters in the +1 oxidation state, their unique Mossbauer hyperfine properties must be due to additional effects such as strong spin-orbit mixing of states or cluster-cluster interactions. It is possible that the cluster nuclearity and/or oxidation state are not those postulated above, and a completely new analysis would be required.

In our present modeling, we have not considered the possible effects of electron delocalization between different layers of the cluster, that is, between the mixed-valence pair and the other ferrous sites. We have found no strong indications that such mixing is present; the σ nature of the electron delocalization within the mixed-valence pair would argue against the importance of this delocalization. However, interlayer resonance effects may be significant in some cases, and this is still under investigation.

To treat the effects of spin-orbit coupling and/or interlayer resonance, one could start with the low-lying eigenstates from the nonlinear model and rediagonalize the appropriate perturbation matrix. This would provide a more concise approach than trying to diagonalize very large matrices de novo.

These two papers demonstrate the scope of a combined exchange-resonance coupling Hamiltonian. The theory has much greater explanatory power for the spin-state energies and (EPR, hyperfine) properties of iron-sulfur clusters than the standard Heisenberg coupling Hamiltonian, and several important physical ideas become apparent. These include the prominent role of electron delocalization (B term) and the countervailing effects produced by a major inequality in the Heisenberg parameters J_2 and J_1 (i.e. where α is small or negative). Both Heisenberg parameters are fairly small, and the Fe^{2+}-Fe^{2+} parameter J_2 may be either antiferromagnetic or ferromagnetic (see P 1). Modest variations in the size of J_1 and J_2 produce a wide variety of spin ground states; the magnitude of B plays an important role by shifting the location in parameter space where spin-state crossings occur. External localizing forces are also very important and show that the protein or cluster environment exerts a very significant effect on the low-lying spin states, a conclusion already apparent from experimental studies.[2,3] Quantitative calculations play an important complementary role to the phenomenological models by determining reasonable ranges in parameter space where state energies and properties should be closely examined, as emphasized in P 1.

Acknowledgment. I thank D. A. Case, P. Yip, E. Munck, J. J. Girerd, V. Papaefthymiou, J. Gaillard, and B. H. Huynh for valuable discussions and the National Institutes of Health (Grant GM39914) for financial support. I also thank J. P. Desclaux for providing the Racah coefficient and matrix diagonalization routines.

(18) Cox, P. A. *Chem. Phys. Lett.* **1980**, *69*, 340.
(19) Girerd, J. J. *J. Chem. Phys.* **1983**, *79*, 1766.

Contribution from the Department of Chemistry, North Dakota State University, Fargo, North Dakota 58105

Sharp-Line Electronic Spectroscopy and Metal-Ligand Geometry in the Pentaamminehydroxochromium(III) Complex

Kyu-Wang Lee and Patrick E. Hoggard*

Received September 14, 1988

The hydroxide ligand is a strong π-donor in metal complexes, and because the interaction is anisotropic, it can cause large perturbations of the t_{2g} subshell. This results in unexpectedly large splittings among the sharp-line transitions in $[Cr(NH_3)_5OH](ClO_4)_2$. The extent of these splittings depends on the orientation of the p orbital on the hydroxide oxygen, which in turn depends on the N-Cr-O-H dihedral angle. Ligand field calculations yielded an estimate of this angle of 20°, approximately midway between an eclipsed and a staggered conformation. The prominent 572 cm^{-1} accepting mode in the luminescence spectrum of $[Cr(NH_3)_5OH](ClO_4)_2$, previously identified with the Cr-O stretching mode, was assigned to the first overtone of the hydroxide internal rotation mode. This overtone is accidentally nearly coincident with a Cr-O-H bending mode in the IR spectrum, but these bands become well separated in spectra of the deuterated complex. The luminescent excited state could be construed as having predominantly $^2A_1$ (^2E_g) character (in C_{4v} and O_h notation).

Introduction

The splittings among the narrow electronic transitions arising within the t_{2g}^3 configuration of pentaammine complexes of chromium(III) have been controversial,[1-4] even following recently reported low-temperature measurements and sophisticated ligand field calculations.[5,6] The splitting of the two $^4A_{2g} \rightarrow {}^2E_g$ components in $[Cr(NH_3)_5X]^{2+}$ (X = Cl, Br, I) complexes is either very small (<20 cm^{-1})[3,5] or unusually large (170-320 cm^{-1}).[1,2,4,6] Very recent resonance line-narrowing experiments favor the latter

(1) Flint, C. D.; Matthews, A. P. *J. Chem. Soc., Faraday Trans. 2* **1973**, *69*, 419.
(2) Shepard, W. N.; Forster, L. S. *Theor. Chim. Acta* **1971**, *20*, 135.
(3) Decurtins, S.; Güdel, H. U.; Neuenschwander, K. *Inorg. Chem.* **1977**, *16*, 796.
(4) Schönherr, T.; Schmidtke, H.-H. *Inorg. Chem.* **1979**, *18*, 2726.
(5) Lee, K.-W.; Hoggard, P. E. *Inorg. Chem.* **1988**, *27*, 907.
(6) Schmidtke, H.-H.; Adamsky, H.; Schönherr, T. *Bull. Chem. Soc. Jpn.* **1988**, *61*, 59.

0020-1669/91/1330-0264$02.50/0